ELSEVIER

Biophysical Chemistry 74 (1998) 135–152

Biophysical Chemistry

Excess counterion binding and ionic stability of kinked and branched DNA

Marcia O. Fenley[a,b], Gerald S. Manning[a,*], Nancy L. Marky[a], Wilma K. Olson[a]

[a] *Department of Chemistry, Rutgers, The State University of New Jersey, Wright-Rieman Laboratories, 610 Taylor Road, Piscataway, NJ 08854-8087, USA*

[b] *Continuum Dynamics, Inc., PO Box 3073, Princeton, NJ 08543, USA*

Received 2 February 1998; received in revised form 28 May 1998; accepted 28 May 1998

Abstract

We compute the excess number of counterions associated with kinked and branched DNA, and the ionic stabilities of these structures as a function of chain length and both sodium and magnesium salt concentration, using numerical counterion condensation theory. The DNA structures are modeled as two or more finite lines of phosphate charges radiating from the kink or junction center. The number of excess counterions around the (40–90°) kinked duplex is very small (at most four). The geometries of large three- and four-way DNA junctions (with > 50 base pairs per arm) in solutions containing low to moderate NaCl concentrations, by contrast, accumulate a substantial number of excess sodium ions (> 20) but no more than 15 magnesium counterions. The excess number of counterions surrounding the kinked linear chain and the branched DNA structures either remains invariant or increases with chain length, tending to reach a plateau value. Open configurations, such as the planar Y-shaped three-way junction (with three 120° inter-arm angles) and the 90° cross-shaped four-way junction, are ionically more stable than compact geometries, such as pyramidal three-way junctions and X-shaped four-way junctions, over the entire range of salt concentration considered (10^{-5}–10^{-1} M NaCl or $MgCl_2$). The ionic stabilities of the compact forms increase with increasing salt concentration and become comparable to those of the extended geometries at high salt (especially when magnesium is the supporting salt). © 1998 Published by Elsevier Science B.V. All rights reserved.

Keywords: Ionic strength; Polyelectrolyte; Counterion condensation theory; Stability; Kinked and branched DNA; Electrostatic; Three- and four-way junction

* Corresponding author. Tel.: +1 732 445 2609; fax: +1 732 445 5312; e-mail: gmanning@rutchem.rutgers.edu

0301-4622/98/$19.00 © 1998 Published by Elsevier Science B.V. All rights reserved.
PII S0301-4622(98)00171-9

1. Introduction

Alternate nucleic acid structures play an important role in biological processes. Proteins, such as SRY, LEF-1 or TBP [1–4], as well as base bulges [5,6] introduce kinks in DNA, dividing the double helix into a two-armed structure. Closely related multi-branched structures [7–10], where three or more duplexes intersect at a single point, serve as possible intermediates in DNA recombination [7,11–13] and important permanent structural elements of naturally occurring RNA molecules [14–16].

Both kinked and branched DNA can be envisioned as sets of polyelectrolyte chains radiating from a common point at the kink or junction center. The close approach of phosphate groups near this site is expected to increase the charge density of such structures compared to linear DNA. Furthermore, the various geometries accessible to both kinked and branched DNA [5,7,17] should give rise to different charge densities. The distinct phosphate charge distributions will, in turn, affect the electrostatic properties of the different configurations, including the distribution of counterions in the vicinity of the kink or junction and the relative ionic stabilities of individual structures.

Until now, only two theoretical studies have provided insight into the accumulation of counterions around kinked and branched DNA. The potentials of mean force calculated for selected atomic configurations yield different three-dimensional distributions of sodium ions around extended square planar and folded X-shaped four-way junctions (FWJ), compared to linear B-DNA at 0.5 M NaCl [18]. More elaborate grand canonical Monte Carlo (GCMC) simulations [19] predict an extra accumulation of sodium ions around a tetrahedral FWJ in aqueous solution containing 1.84 mM NaCl, and an increase in the number of excess sodium ions associated with structures of increasing chain length until reaching a plateau value (of ~ 24). Under identical ionic conditions, the GCMC computations find approximately the same number of excess sodium ions in the vicinity of a 90° cross-shaped four-way junction and a tetrahedral structure, but a much larger number of excess sodium ions around an idealized and more compact X-shaped junction with two acute angles of 20°.

Four-way DNA junctions undergo a salt-dependent conformational transition from an unfolded square-planar configuration at low salt to a folded X-shape at sufficiently high salt [5,7,20]. The long-range electrostatic repulsions between the negatively charged DNA phosphates presumably dominate at low salt concentrations, and favor extended and unfolded branched structures with smaller charge densities [5,7]. At sufficiently high salt concentrations, when electrostatic repulsions are substantially reduced, compact and folded forms with higher charge densities should compete with the open structures. Significantly, magnesium and more highly charged cations are better than sodium in inducing folded arrangements of four-arm DNA junctions [20,21]. A smaller concentration of the cation with higher charge stabilizes the folded form compared to the ion with lower charge.

In this paper we report on the number of excess counterions and the ionic stabilities of kinked and branched DNA for varying chain lengths and salt concentrations obtained with numerical counterion condensation theory [22]. These simple and fast calculations allow us to address a broader range of branched structures, chain lengths and ionic conditions than can be addressed with the much more computationally demanding procedures reported previously [18,19]. Here we consider magnesium as well as sodium counterions surrounding a variety of different kinked and branched geometries over a broad range of salt concentration and chain length. Unlike GCMC computations, numerical counterion condensation theory is not subject to large computational uncertainties. Both approaches, however, are based on a similar DNA model, where the phosphates are placed on finite lines which meet at the kink or junction center, and both share the limitation of providing only the average number of associated counterions. Thus, we can compare our results against the GCMC simulations for the same DNA structure under identical ionic conditions. The paper is organized as follows. In Section 2 we describe our DNA model

and methodology, which allow us to examine the excess counterion binding and ionic stabilities of kinked and branched DNA over a broad range of salt (both sodium and magnesium) concentration and chain length. Then, in Section 3 we present our findings and compare them against relevant theoretical and experimental work. Finally, in Section 4 we summarize the general trends in our data and provide suggestions for further work.

2. Model and method

2.1. DNA representation

In order to examine the accumulation of counterions around different configurations of kinked and branched DNA and to estimate their relative ionic stabilities, we adopt a simplified model where the overall negative residue charge is concentrated at the phosphorus (P) atoms and the phosphorus positions are projected on the helical axis. The linear segments, which meet at the kink or branch center, crudely incorporate features of the local conformation.

2.1.1. Axial phosphate charge model

The assumed 1.7-Å separation of most negative charges corresponds to the average spacing on the helical axis of phosphate groups from complementary strands of the B-DNA duplex [23]. We account for the possible distortion of phosphate positions near the kink or junction site by varying the charge spacing of the centrally located charges in an ad hoc fashion consistent with currently available structural information. For example, B-DNA helical parameters are usually altered within five base pair (bp) steps of the kink site in severely distorted protein–DNA complexes [17] and the arms of three- and four-way DNA junctions adopt normal B-form conformations right up to the junction base pairs [24–26].

We consider both larger and smaller charge spacing near the kink or junction region in order to account for the possible extension or compression of phosphate groups around the kink or branch site. For most of the calculations we keep adjacent phosphates 1.5 Å from the kink or junction. This positioning, which spreads the phosphates apart compared to ideal B-DNA, mimics the stretching implicated in the sharp kinking of DNA by TBP [27]. We also consider the axial charge spacing adopted in GCMC calculations [19] where the central phosphates are placed 0.85 Å from the kink/junction center and the next neighbors are displaced an additional 3 Å along each arm.

The number of counterions bound to kinked and branched DNA and the associated ionic free energy are not significantly affected by changes in charge spacing near the kink or junction region (results not shown). The computed values are practically invariant to the spacing of the centrally located phosphates in long structures at high salt concentrations and/or in the presence of multi-valent cations (e.g. magnesium) due to their smaller effect on larger structures and the better screening of electrostatic repulsions under these ionic conditions.

2.1.2. Kinked and branched DNA geometries

For planar kinked DNA we consider a broad range of bending angles (40, 90, 140°), consistent with known deformations of DNA kinked by proteins [1–4] and base bulges [5,6]. The bending angle θ is defined as the complement of the angle between the two helical arms ($\theta = 0°$ for the straight duplex). Thus, we consider kinked DNA with an obtuse angle as well as less pronounced kinked structures. The kink site is located in the center of our ideal models and, unlike crystallographically based models [28], there is no displacement of the two converging helical axes.

For the perfect three-arm DNA junctions (with no unpaired bases) we consider four planar geometries: (1) a threefold symmetric Y-shape with arms radiating to points that define an equilateral triangle, i.e. with three 120° inter-arm angles; hereafter referred to as the Y-shape (120°); (2) a twofold symmetric Y-shape with an acute angle of 60° between two arms and two angles of 150° between the other adjacent arm pairs; hereafter referred to as the Y-shape (60°); (3) an asymmetric 'y' with three different inter-arm angles, i.e. 20°, 160° and 180°; hereafter referred to as the 'y'-shape; and (4) a T-shaped form with two inter-arm angles of 90°. We also study two non-

planar geometries: (1) a trigonal pyramid with three 60° inter-arm angles; termed the pyramid (60°); and (2) a pyramidal form with three 90° inter-arm angles called the pyramid (90°). All six geometries have been suggested by different experimental studies [29–33].

For the four-way DNA junctions the following geometries are considered: (1) an ideal tetrahedral form with inter-arm angles of 109°; (2) two twofold symmetric planar X-shapes, one with two inter-arm angles of 20° and another with two inter-arm angles of 60°; hereafter referred to, respectively as the X-shape (20°) and X-shape (60°); (3) a planar cross-shaped structure with four inter-arm angles of 90°, also called square-planar; and (4) an asymmetric form, a distorted tetrahedral structure where one of the arms is reflected by 180° with respect to the geometrical center of the structure. These geometries have also been suggested by experimental work [20,34,35].

Fig. 1 illustrates the distribution of phosphate charges in the assumed geometries of the two-arm kinked DNA and the three- and four-way junction structures, all with 10 bp/arm. The average interphosphorus distances and the radii of gyration of various two-armed kinks and three- and four-way junctions with 20 bp branches are reported in Table 1. The mean P–P values tend in most cases to increase with increasing radius of gyration (a measure of the molecular compactness). The average phosphate distances of the tetrahedral four-way junction, however, are greater than expected on the basis of the radius of gyration.

2.2. Condensed counterion fraction and ionic free energy

We now briefly review the method employed to compute the fractional number of condensed counterions and the ionic free energy of the DNA-counterion-solvent system, which is based on the framework of numerical counterion condensation theory [22]. According to classical counterion condensation theory [36], the overall free energy associated with DNA immersed in an aqueous solution of electrolytes (termed the ionic

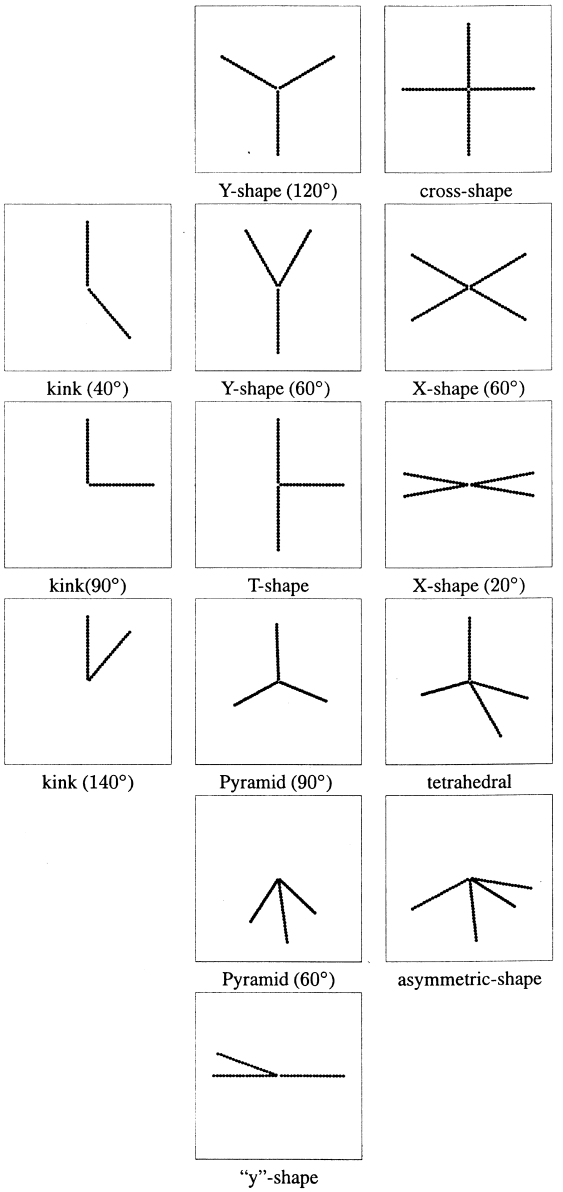

Fig. 1. Schematic showing phosphorus positions in the various configurations of the two-arm DNA kinks, and the three- and four-arm DNA junctions studied here. The reader is referred to the text for a description of the angles between the arms of both kinked and branched DNA molecules here shown (see Section 2.1.2).

or polyelectrolyte free energy), G_{ionic}, is expressed as:

$$G_{\text{ionic}} = G_{\text{elec}} + G_{\text{mix}}, \tag{1}$$

Table 1
Radii of gyration R_g and average phosphorus–phosphorus (P–P) distances ⟨P–P dist⟩ for different configurations of two-arm DNA kinks and three- and four-way DNA junctions[a]

Configuration	R_g (Å)	⟨P–P dist⟩ (Å)
Kinks		
(140°)	22.8	28.6
(90°)	31.2	38.0
(40°)	37.8	44.6
Three-way junctions		
Pyramid (60°)	27.9	35.6
Pyramid (90°)	34.2	42.9
'y'-shape	37.9	44.3
T-shape	37.9	46.6
Y-shape (60°)	38.7	46.9
Y-shape (120°)	39.6	48.8
Four-way junctions		
Asymmetric shape	34.7	43.6
X-shape (20°)	39.6	46.9
Tetrahedral	38.8	48.5
X-shape (60°)	39.6	48.9
Cross shape	39.6	49.5

[a]All structures have 20 bp/branch.

where the first term represents the free energy associated with electrostatic repulsions of the charged phosphate groups and the second term is the ideal free energy of mixing condensed counterions, free counterions and solvent molecules.

The electrostatic energy of the system, G_{elec}, assumes that electrostatic interactions between all pairs of phosphate charges can be described by a screened Debye–Hückel potential. In order to treat DNA of any configuration and length, G_{elec}, can be written as:

$$\sum_{k<j}^{N_p} (q_{\text{net}})^2 \frac{e^{-\kappa r_{kj}}}{\varepsilon r_{kj}}, \tag{2}$$

where N_p is the total number of phosphate groups, r_{kj} is the distance between the kth and jth phosphate groups and ε is the dielectric constant of water at 298 K (i.e. 78.3). The net or effective charge of each negatively charged phosphate group, q_{net}, is given by:

$$q_{\text{net}} = q(1 - N\theta_N), \tag{3}$$

a term which reflects the counterion condensation phenomena (i.e. each phosphate charge is reduced from q to q_{net} by counterion condensation). The parameter θ_N is the number of bound counterions of valence N per phosphate charge on DNA (i.e. the fractional number of condensed counterions) and q is the magnitude of the elementary charge. The Debye–Hückel screening parameter, κ, is proportional to the square root of the salt concentration, c_s.

The ideal free energy of mixing free counterions, bound counterions and solvent molecules is expressed as:

$$G_{\text{mix}} = N_p \theta_N RT \ln\left(\frac{10^3 \theta_N}{c_s \upsilon}\right), \tag{4}$$

where υ is the condensation volume per mole of phosphate (i.e. volume surrounding the DNA within which the N-valent counterions are considered bound), R is the universal gas constant, and T is the temperature, taken as 298 K. For the NaDNA/NaCl and MgDNA/$MgCl_2$ systems, the respective values of υ, obtained for the infinite line model of B-DNA in the limit of zero salt concentration [36], are 646 and 1121 cm^3/mol phosphate. We assume that these values of υ are independent of the configuration and size of DNA as well as the particular salt concentration.

We employ the B-DNA value of υ for both kinked and branched DNA structures since the distortions caused by the kink or junction region do not significantly alter the B-type conformation in the kink/junction region [17,24–26]. However, it should be pointed out that the influence of the distribution of phosphate charges at the kink or junction site on υ is not considered (i.e. for kinked and branched DNA two or more lines of phosphate charges converge at a center point whereas there is only a straight line of charges in the original CC model).

Some comments should be made about the above equations. First, in Eq. (2) the Debye–Hückel interaction is a better approximation for distant pairs than for close pairs of phosphates. Nevertheless, the use of self-consistently calculated effective phosphate charges ame-

liorates the approximation even for close pairs. It may be recalled as well that in some situations, charges on a line interacting with a bulk dielectric constant mimics the behavior of a more realistic charge distribution used with a locally saturated dielectric constant [22]. In this sense, local solvent effects are partially taken into account. We are unable to provide a meaningfully quantitative a priori estimate of the range of validity of Eq. (2). Approximations of this nature are best controlled by comparison with experimental and simulated data, as we subsequently provide. Second, Eqs. (1)–(4) and the definition of κ assume that the salt concentration is much greater than the concentration of phosphate charges. Our system consists of a NaDNA (or MgDNA) salt immersed in a NaCl (or $MgCl_2$) solution of molarity c_s. Third, only the contributions to the ionic free energy that are dependent on θ_N are considered, since other terms cancel in free energy differences or derivatives. Fourth, the delocalized or territorial mode of counterion binding is assumed. There is experimental support for this mode of ion binding to branched DNA structures [5,20].

In order to obtain the equilibrium or average value of θ_N one must minimize G_{ionic}, given by Eqs. (1)–(4), with respect to θ_N. This is accomplished by equating the derivative of G_{ionic} with respect to θ_N to zero and finding the root of the equation, $(\frac{\partial G_{\text{ionic}}}{\partial \theta_N}) = 0$, where,

$$\left(\frac{\partial G_{\text{ionic}}}{\partial \theta_N}\right) = -2Nq^2(1-N\theta_N)\sum_{k<j}^{N_p}\frac{e^{-\kappa r_{kj}}}{\varepsilon r_{kj}} + N_p RT\left[1+\ln\left(\frac{10^3\theta_N}{c_s \upsilon}\right)\right]. \quad (5)$$

The value of θ_N at equilibrium is determined numerically using the Newton–Raphson method [37]. We should point out that θ_N of kinked or branched DNA represents an average for a particular distribution of phosphate charges; the phosphates near the kink or junction region and those far out along the arms contribute equally. We therefore obtain only an overall value of θ_N from the above minimization procedure.

From the value of θ_N and υ one can compute the excess number of counterions due to the kink/junction region and the ionic free energy differences (in kcal/mol) between different kinked/branched DNA structures. The latter quantities provide information about the relative ionic stabilities of different configurations of kinked and branched DNA. For a more complete discussion of the underlying assumptions and methodology the reader is referred elsewhere [22]. In the following section we define the number of excess counterions associated with kinked and branched DNA structures. This quantity relies on the specification of a reference state.

2.3. Kinked / branched DNA reference states

For kinked DNA the reference state is a straight DNA chain with the same number of phosphate groups. Therefore the number of excess counterions due to the kink is given by:

$$N_{\text{kink}}(\text{excess}) = N_p[\,\theta(\text{kink}) - \theta(\text{straight})] \quad (6)$$

where N_{kink}(excess) is the number of excess counterions due to the kink in DNA, N_p is the total number of phosphate groups, θ(kink) and θ(straight) are the respective counterion binding fractions for kinked DNA and straight B-DNA. The products $N_p\theta$(kink) and $N_p\theta$(straight) give the total number of counterions associated or bound to kinked and straight DNA, respectively.

For the three-arm DNA junctions, the reference state is three DNA helices with the same total number of phosphate groups as the three-arm DNA junction (each helix has the same number of phosphate groups as one of the arms of the three-arm junction). Thus, the number of excess counterions associated with a three-way junction (TWJ) is given by:

$$N_{\text{TWJ}}(\text{excess}) = N_p[\,\theta(\text{TWJ}) - \theta_{\text{one-arm}}(\text{straight})] \quad (7)$$

where N_{TWJ}(excess) is the number of excess counterions associated with the TWJ, θ(TWJ) is the counterion binding fraction of the TWJ and

$\theta_{\text{one-arm}}$(straight) is the corresponding counterion binding fraction for straight B-DNA with the same number of phosphate groups as one of the arms of the TWJ.

For the four-arm junction we can define the number of excess counterions in two ways. The reference state can be either four or two helices with the same total number of phosphate groups as the FWJ. In the former case each helix corresponds to one of the arms of the FWJ and in the latter case to two coaxial arms of the structure. Our results (data not shown) show that, as expected, there are more excess counterions at the junction if we use the four helix reference. Both reference states have been used in past thermodynamic studies of DNA branching [10]. Here we choose the two helix case, which gives a lower bound on the excess junction counterions, in order to compare our results with earlier GCMC computations [19]. Consequently, the number of excess counterions associated with the FWJ is defined as:

$$N_{\text{FWJ}}(\text{excess}) = N_p[\,\theta(\text{FWJ}) - \theta_{\text{two-arms}}(\text{straight})] \quad (8)$$

where N_{FWJ}(excess) is the number of excess counterions associated with the FWJ, θ(FWJ) is the counterion binding fraction of the FWJ and $\theta_{\text{two-arms}}$(straight) is the corresponding counterion binding fraction for straight B-DNA with the same number of phosphate groups as two of the arms of the FWJ.

In the following sections we employ numerical counterion condensation theory (NCCT) [22] to compute the excess counterion accumulation and ionic stability of several different kinked and branched DNA structures over a broad range of salt (both sodium and magnesium) concentration and arm lengths. Whenever possible we compare our results with GCMC predictions [19] as well as with relevant experimental findings.

3. Results and discussion

3.1. Kinked DNA

We first examine the number of counterions surrounding a kinked DNA duplex compared to an ideal B-DNA. Table 2 gives the number of sodium and magnesium ions associated with 140- and 90°-kinked DNAs and with the linear reference state at two different salt concentrations (i.e. 10^{-3} and 10^{-1} M) and six chain lengths (10–200 bp). At moderate salt concentrations, there is an extra accumulation of sodium ions around the severely kinked (140°) DNA relative to B-DNA. However, for all fragments (up to 200 bp) and salt concentrations the number of excess sodium ions

Table 2
Chain length and ionic strength dependence of the number of associated sodium and magnesium ions for kinked and straight DNA in aqueous solutions[a]

Number of base pairs per kink	Number of associated counterions	
	Kinked DNA	B-DNA
$c_s = 10^{-3}$ M, Sodium		
10	13.7 (12.6)	12.4
20	29.3 (27.8)	27.3
40	60.9 (58.5)	57.7
60	92.4 (89.3)	88.3
100	155.2 (150.8)	149.4
200	310.0 (304.0)	302.4
$c_s = 10^{-1}$ M, Sodium		
10	15.8 (14.9)	14.8
20	31.6 (30.5)	30.3
40	62.8 (61.4)	61.3
60	93.7 (92.4)	92.2
100	155.6 (154.2)	154.2
200	310.4 (308.8)	308.8
$c_s = 10^{-3}$ M, Magnesium		
10	8.6 (8.3)	8.3
20	17.6 (17.2)	17.0
40	35.4 (34.9)	34.7
60	53.3 (52.6)	52.3
100	88.8 (88.0)	87.6
200	177.2 (176.0)	176.0
$c_s = 10^{-1}$ M, Magnesium		
10	9.0 (8.8)	8.8
20	18.0 (17.8)	17.8
40	35.9 (35.7)	35.7
60	53.8 (53.5)	53.5
100	89.6 (89.4)	89.2
200	178.8 (178.8)	178.8

[a] The numbers in parentheses refer to the 90°-kinked DNA and those without parentheses are for the 140°-kinked DNA.

is small compared to the total number of sodium ions surrounding the kink. At high salt (10^{-1} M NaCl), the number of excess sodium ions is even smaller, at most two for all kinked DNA geometries. As expected from the average phosphorus–phosphorus distances, the more widely spaced charges in the 90° kink attract fewer counterions compared to the 140° kink in DNA of the same length (see Table 1). For the 40°-kinked DNA (at all chain lengths) and 90°-kinked DNA (for small fragments < 100 bp) at any salt concentration, there are no extra sodium ions accumulated near the kinked DNA.

The build-up of sodium ions around 90° and 140° kinks is seen more clearly in Fig. 2 where the number of excess counterions is plotted as a function of chain length for different ionic conditions. We see that the accumulation of sodium tends to reach a plateau at long chain lengths and that the number of excess ions decreases at higher salt concentration. The latter trend reflects the salt dependence of the counterion binding fraction of both straight and kinked DNA, both of which decrease with increasing salt concentration at a fixed and finite chain length [22].

The effect of the kink is more pronounced for smaller molecules in spite of the fact that fewer excess sodium ions associate with them. For example, at 10^{-3} M NaCl, the 140°-kinked DNA of 10 bp has 0.067 excess sodium ions per phosphate group, whereas the corresponding ratio for the 140°-kinked DNA of 60 bp is 0.034 excess. This trend persists for all kinked DNA structures regardless of salt concentration.

As shown in Table 2, increasing the charge of the supporting salt significantly decreases the number of excess counterions due to the kink region at all salt concentrations and chain lengths. The difference in the number of excess magnesium and sodium counterions is largest at the low salt end. At intermediate salt concentrations (10^{-3} M), there are practically no excess magnesium ions even for the pronounced 140°-kinked DNA. For 90- and 140°-kinked DNA structures of any chain length the excess number of magnesium ions is no more than three regardless of salt concentration. As in the case of sodium, the number of excess magnesium ions due to the kink

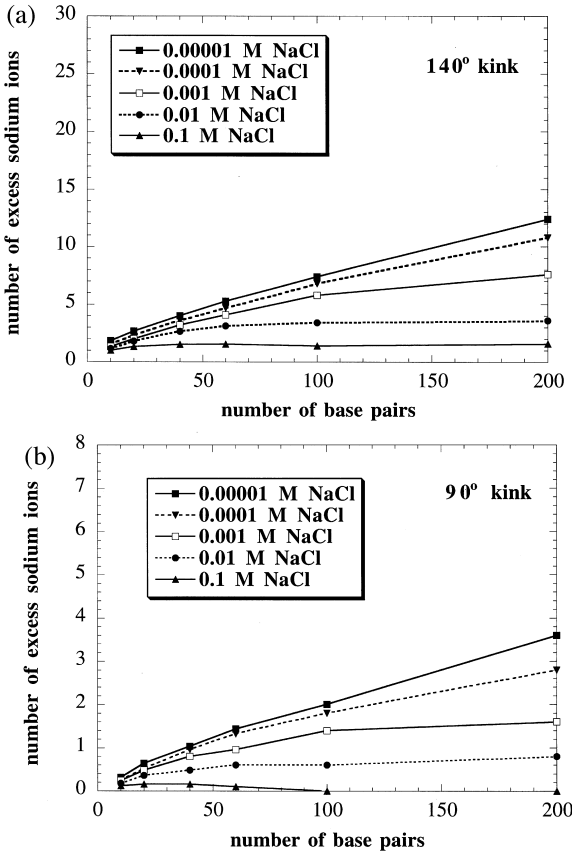

Fig. 2. Chain length dependence of the excess number of sodium ions accumulated around (a) 140°; and (b) 90° kinks in the center of a B-DNA fragment at different NaCl concentrations.

increases with increasing chain length. Plateau values, where the number of excess magnesium ions is invariant to changes in chain length, are reached at moderate to high salt concentrations.

In summary, the number of excess counterions (sodium or magnesium) for $\leq 90°$ pronounced kinked DNA molecules is very small and thus, the counterion distribution around DNA with < 100 bp is probably unaffected by bending angles smaller than 90°. However, one should keep in mind that for more pronounced kinks in larger DNA fragments at the low salt end, the counterion distribution could possibly differ from straight DNA, reflecting a larger accumulation of ions due to the kink site (i.e. larger average extent of counterion condensation).

3.1.1. Comparison with GCMC simulations

For the case of 60 bp DNA with a 70.5° kink (109.5° inter-arm angle) at 0.0018 M NaCl we obtain 0.2 excess sodium counterions due to the kink, a value in reasonable agreement with the 1.1 excess sodium found by Olmsted and Hagerman [19] with GCMC computations of the same kink under identical ionic conditions. Both studies show that there is practically no extra accumulation of ions due to this kink. We obtain even closer agreement with Olmsted and Hagerman [19] for a more pronounced 160°-kinked DNA (20° inter-arm angle) of the same length and at the same salt concentration; we obtain 6.9 excess sodium counterions, whereas they obtain a value of 7.0. The two approaches agree that there is an extra accumulation of sodium ions around pronounced DNA kinks. Note, however, that our values for the excess kink counterions are smaller in both cases than those computed by GCMC simulations. Actually, the definitions of bound counterions differ in the two approaches, and are not directly comparable. The number of bound counterions in the GCMC simulation includes the non-ideal screening effect of the diffuse Debye–Hückel atmosphere in addition to the condensed counterions [38], whereas counterion condensation theory counts as bound only the condensed counterions.

3.1.2. Smoothly bent vs. kinked DNA

We have previously shown that there is some extra accumulation of counterions around smoothly bent DNA (only for cases where the bending angle is large and at the low salt end) [39]. For example, for a 60-mer at 10^{-4} M NaCl with a 45-Å radius of curvature (which corresponds to a uniform bending angle of 4.3° per base-pair), the number of associated counterions is $0.713 \text{ ions/bp} \times 120 \text{ bp} = 85.6$ ions, whereas, there are $0.701 \text{ ions/bp} \times 120 \text{ bp} = 84.1$ counterions for the B-DNA linear reference. Thus, there is an excess of approximately two counterions around smoothly bent DNA. For an equivalently kinked (130°) DNA of the same chain length, there are approximately four counterions in excess at 10^{-4} M NaCl. Therefore there are a few more counterions surrounding a kink as opposed to a smooth bend of the same overall magnitude.

3.1.3. Ionic stability of kinked vs. straight DNA

The energetic cost (considering only the ionic contribution) involved in kinking DNA under different ionic conditions is reported in Fig. 3. The ionic free energy difference between 20-bp kinked and straight DNA is plotted as a function of the concentration of both NaCl and $MgCl_2$. The decrease to zero of the ionic stability curves at high salt occurs more quickly for the less pronounced kinked DNA structure (e.g. compare the 140° vs. 90° curves). For less pronounced kinked DNA molecules in either NaCl or $MgCl_2$ solutions the ionic free energy difference between kinked and straight DNA is < 3 kcal/mol at all salt concentrations. However, for severely (140°) kinked DNA, the ionic free energy difference is higher than 10 kcal/mol at the low NaCl end. At all salt concentrations and regardless of salt charge, the 90°-kinked DNA is always ionically more stable than the 140°-kinked DNA. The ionic free energy cost to kink a straight DNA fragment in solutions of $MgCl_2$ becomes very small at high salt concentrations. For example, the ionic free energy difference between straight DNA and the 140°-kinked DNA is approx. 0.2 kcal/mol at 10^{-1} M $MgCl_2$. Thus, even for the most pronounced DNA kinks, one can deform DNA at high ionic conditions without much barrier in terms of the ionic component of the total bending free energy. On the other hand, at low ionic conditions the ionic contribution to the total free energy of bending is significant for the more pronounced kinked DNA (especially when sodium is the counterion).

3.2. Three-way DNA junctions

In Table 3 we present the chain length dependence of the number of associated sodium counterions for two representative geometries of three-way DNA junctions and their linear reference states at 10^{-3} and 10^{-1} M NaCl. As evident from the data, the non-planar pyramid (60°) accumulates a larger number of counterions compared to the Y-shape (120°). The former structure

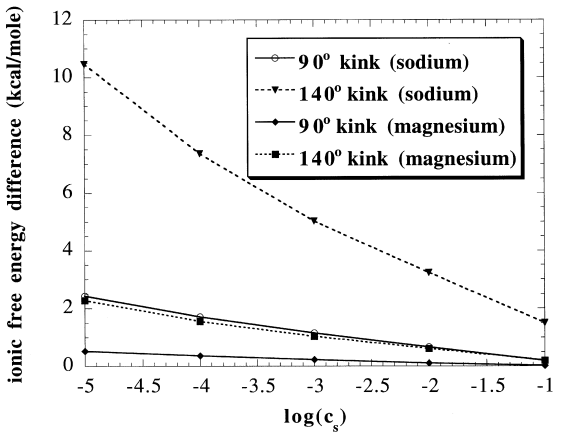

Fig. 3. Dependence of the ionic free energy differences between (90° and 140°) kinked and straight DNA on c_s, the concentration of salt (NaCl and $MgCl_2$) in molarity units.

is significantly more compact than the latter configuration according to Table 1 with the average P–P distance and radius of gyration of the pyramid (60°) ~30% lower than the corresponding values of the Y-shape (120°). Thus, as expected, the more compact pyramid (60°) with the larger charge density and stronger electrostatic repulsions accumulates the larger number of excess junction counterions. Nevertheless, there is an uptake of sodium ions for all TWJ geometries (more so at low salt concentration and for larger TWJs). The charge densities of the branched structures are consistently higher than those of linear DNA due to the fact that the phosphate groups come into close proximity upon formation of the junction.

The predicted chain length and ionic strength dependencies of the number of excess sodium ions for various TWJ geometries in Fig. 4 resembles general features seen above for kinked linear DNA. For all geometries the excess number of sodium ions increases with increasing arm length and decreasing salt concentration. At 10^{-5} M NaCl, the excess number of sodium ions is about the same for the two Y-shaped forms, the pyramid (90°) and the T-shape (with up to 20 bp/arm), but is larger for the pyramidal (60°) and 'y'-shaped geometries, which coincide in Fig. 4a. The differences are slightly more pronounced (10–15 ions) in TWJs with longer arms at this salt concentration. The relative effect of the junction on cation

Table 3
Arm length and ionic strength dependence of the number of associated sodium counterions around Y-shaped and pyramidal three-way DNA junctions in aqueous solution[a]

Number of base pairs per arm	Number of associated counterions	
	TWJ DNA Junction	B-DNA
Y-shape (120° inter-arm angles)		
5	20.5 (22.9)	15.3 (21.0)
10	43.9 (46.2)	37.1 (44.4)
20	90.6 (92.6)	82.0 (91.0)
30	137.2 (139.1)	127.4 (137.3)
50	229.8 (231.9)	219.0 (230.1)
100	459.6 (464.4)	448.2 (462.6)
Pyramid (60° inter-arm angles)		
5	22.1 (24.3)	15.3 (21.0)
10	46.2 (48.1)	37.1 (44.4)
20	94.4 (94.7)	82.0 (91.0)
30	142.4 (141.1)	127.4 (137.3)
50	237.0 (234.0)	219.0 (230.1)
100	469.8 (466.5)	448.2 (462.6)

[a]The numbers in parentheses refer to 10^{-1} NaCl concentration and those without parentheses to 10^{-3} M NaCl.

association, however, is more pronounced for smaller junctions since the number of excess counterions on a per phosphate basis is larger.

The number of excess sodium ions around all TWJ geometries is still significant (10–30 ions) at moderate (10^{-3} M) NaCl concentration; see Fig. 4b. Also, under these ionic conditions there are more excess sodium ions associated with the more compact geometries, e.g. pyramid (60°). On the other hand, we see that under high (10^{-1} M) NaCl concentrations the number of excess counterions due to the junction is small for TWJs of any geometry (at most around six); see Fig. 4c.

As in the case of kinked DNA, the number of excess magnesium ions at the different junctions is smaller than the amount of excess sodium at a fixed salt concentration and chain length (note the different scale in Fig. 5 compared to Fig. 4). Furthermore, the amount of excess magnesium is comparable (0–4 ions) for extended and compact forms, i.e. Y-shaped (120°) vs. pyramidal (60°) TWJs, at all chain lengths and for moderate to high salt concentrations. This is in contrast to the

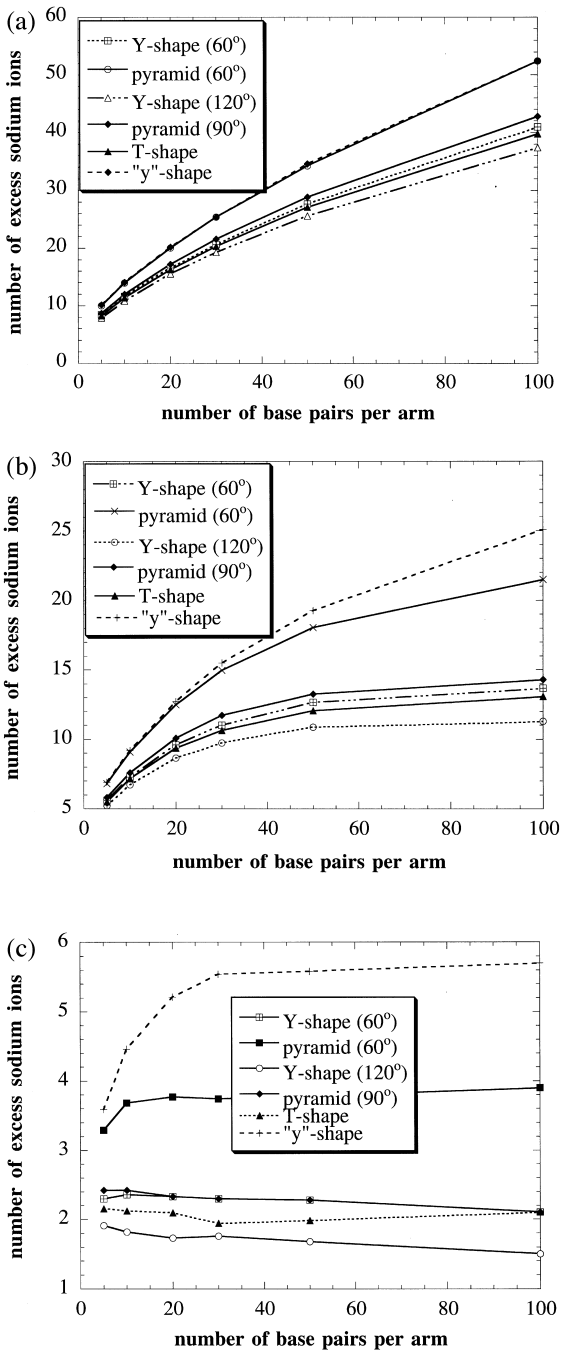

Fig. 4. Chain length dependence of the excess number of sodium ions accumulated around different configurations of three-way DNA junctions in aqueous (a) 10^{-5} M; (b) 10^{-3} M; and (c) 10^{-1} M NaCl solution.

case where sodium is the counterion. At 10^{-1} M $MgCl_2$, there are practically no excess counterions around any three-way junction regardless of the number of base pairs per arm, and at 10^{-3} M the limiting values of the excess magnesium ions are approximately two for configurations other than the pyramidal (60°) and 'y'-shaped structures where the excess is 4–5 counterions.

3.2.1. Ionic stability of three-way junctions

Some experimental studies have shown that ionic strength effects (both ion charge and concentration) assume an important role in stabilizing perfect TWJs [30,31], while others find that

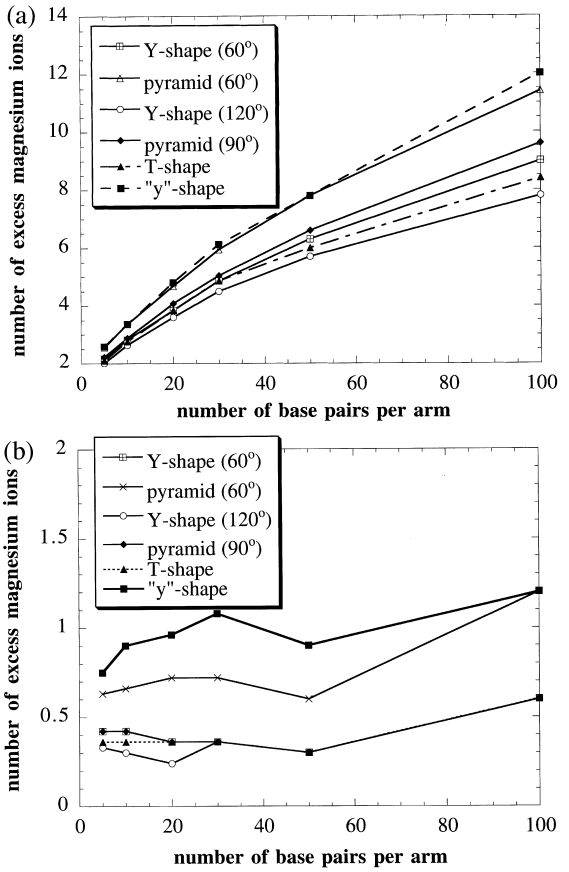

Fig. 5. Chain length dependence of the excess number of magnesium ions accumulated around different configurations of three-way DNA junctions in aqueous (a) 10^{-5} M; and (b) 10^{-1} M $MgCl_2$ solution.

salt plays no role [29,32]. Gel electrophoretic and thermodynamic studies [40–44] on bulged DNA and RNA TWJs show that there is a salt-induced transition from an extended or open configuration in the absence of added ions to a compact asymmetric structure in the presence of metal ions (e.g. magnesium or hexammine cobalt). The predicted free energy differences between symmetric Y-shaped TWJs and various distorted forms can shed light on these observations.

The relative ionic stabilities of 20 bp/arm TWJs plotted in Fig. 6 reveal an ordering of stability not obvious from the radii of gyration and average P–P distances. The symmetric Y-shaped (120°) TWJ is ionically more stable than all other configurations with the ionic free energy differences, relative to the Y-shape (120°), decreasing in the following order: 'y'-shape ≈ pyramid (60°) > pyramid (90°) > Y-shape (60°) > T-shape. At the high salt end (10^{-1} M NaCl), the stability of the Y-shaped (60°), T-shaped and pyramidal-shaped (90°) TWJs approach that of the symmetric Y-shape (120°) with ionic free energy differences less than 0.8 kcal/mol. On the other hand, at the same salt concentration, the ionic stabilities of the 'y'-shaped and pyramidal (60°) TWJs are still much less than that of the Y-shape (120°). For longer (100 bp/arm) TWJs the ionic stability follow the same order, but the ionic free energy differences are larger (especially at low NaCl conditions).

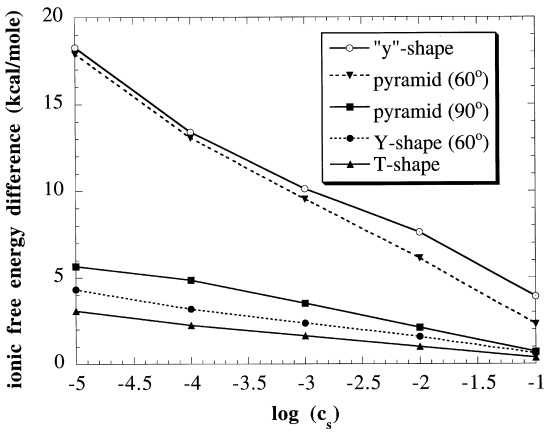

Fig. 6. Ionic free energy differences between various three-way (20 bp arms) DNA junctions and the ideal Y-shaped configuration as a function of the logarithm of the NaCl concentration, c_s.

The ionic free energy differences are much smaller when magnesium is the supporting salt. For instance, the respective ionic free energy differences between the 10 bp/arm T-shape and extended Y-shape (120°) are 0.3 and 0.01 kcal/mol at 10^{-1} M NaCl and $MgCl_2$. However, the order of ionic stability remains the same as that in sodium. Thus, the order of ionic stability is independent of both salt concentration and charge. In contrast to NaCl solutions, the ionic stability of all configurations become comparable to the Y-shape (120°) TWJ at high magnesium concentrations. The ionic free energy differences between all geometries and the symmetric Y-shape (120°) are < 0.6 kcal/mol at 10^{-1} M $MgCl_2$. Thus, even the more compact TWJ geometries are ionically equivalent to the extended forms at high magnesium concentration.

In conclusion, our results show that the ionic stabilities of TWJs are affected by the concentration and charge of metal ions present in solution and thus suggest that ionic strength effects play a role in determining the overall stability of TWJs. Clearly, the charge density of the TWJ is large, since one has three polyelectrolyte chains converging at the junction site, inducing considerable electrostatic repulsions between phosphates. Consequently, the stability of the TWJ, like that of linear DNA, is sensitive to the ionic environment. For instance, under low salt conditions (especially for sodium), the ionic free energy contribution is large and probably prevents compact TWJs from occurring. Thus, the angle between the different pairs of arms of the TWJ is probably dictated in part by the ionic conditions. On the other hand, provided that all other contributions to the total free energy difference are also small, more than one geometry of small TWJs can probably co-exist under moderate $MgCl_2$ concentrations. The ionic free energies of competing configurations differ by as little as 0.1 kcal/mol.

3.2.2. Comparison with experiments

Our prediction that the extended Y-shaped (120°) TWJ is the most stable configuration (assuming that the ionic free energy dominates all

other free energy contributions) under low salt conditions is supported by gel electrophoretic mobility and fluorescence studies [29,32]. At low salt concentrations, where the ionic free energy is dominant, only extended or open TWJ geometries like the 120° Y-shape are probably stable. Our results also show that the 120° Y-shape is ionically more stable than all other geometries over the entire range of salt concentration (for both sodium and magnesium) in agreement with gel electrophoretic and fluorescence studies [29,32]. It should be pointed out that these experimental studies are also consistent with non-planar pyramidal geometries, since the data support a structure with three equal inter-arm angles (which might be different from 120°). Non-planar pyramidal geometries, however, are more compact than the planar Y-shape form (see Table 1) and according to our calculations are not likely to be stable at low salt conditions.

A cyclization method coupled with two-dimensional gel electrophoresis analysis [33] of perfect three-arm junctions, made up of a duplex stem and hairpin in one arm and two linear arms with sticky ends, in the presence of 10 mM $MgCl_2$ suggests that the TWJ adopts a pyramidal geometry with equal inter-arm angles in the range 60–90°. This study relies on the assumption that the spatial arrangements of DNA TWJs in linear and circular molecules are the same, based on the similar electrophoretic mobilities of linear and closed circular molecules with the three-way construct. According to our results, at 10^{-1} mM $MgCl_2$ the respective ionic free energy differences between the pyramidal (90°) and (60°) forms are 0.3 kcal/mol and 0.8 kcal/mol relative to the extended 120° Y-shape (all with 10 bp/arm). Thus, since small ionic free energy differences are involved at such ionic conditions, other contributions to the total free energy could stabilize a pyramidal form.

Gel electrophoretic mobility and chemical and enzymatic footprinting studies [30] further suggest that the TWJ adopts an asymmetric configuration (e.g. T-shape) in the presence of metal ions, such as magnesium. Our results show that the ionic free energy differences between the 30 bp T-shaped and extended Y-shaped (120°) structures are 0.1 and 0.04 kcal/mol at 10^{-2} M and 10^{-1} M $MgCl_2$, respectively, suggesting that the two geometries are energetically equivalent. Thus, under high salt conditions more than one geometry may be energetically accessible, and there could be a dynamic exchange between different configurations of TWJs (i.e. a family of equilibrium structures). At such salt conditions, the stacking interactions (or other non-ionic interactions) may be dominant and dictate which overall structure is more favorable.

3.3. Four-way DNA junctions

The salt and chain length dependent trends seen in the electrostatic properties of kinked and three-way branched DNA persist in the analysis of four-way junctions. At high (0.1 M NaCl) salt

Table 4
Arm length and ionic strength dependence of the number of associated sodium ions around different four-way DNA junctions in aqueous solution[a]

Number of base pairs per arm	Number of associated counterions	
	FWJ DNA	Junction B-DNA
Cross-shape		
5	29.7 (31.8)	24.8 (29.6)
10	61.8 (63.2)	54.6 (60.6)
20	125.9 (125.1)	115.4 (122.6)
30	189.4 (187.2)	176.6 (184.6)
50	314.4 (310.8)	298.8 (308.4)
100	622.4 (620.0)	604.8 (617.6)
Tetrahedral		
5	29.9 (32.0)	24.8 (29.6)
10	62.2 (63.4)	54.6 (60.6)
20	126.4 (125.6)	115.4 (122.6)
30	190.1 (187.4)	176.6 (184.6)
50	315.6 (311.2)	298.8 (308.4)
100	624.0 (620.8)	604.8 (617.6)
X-shape (60°)		
5	30.0 (32.1)	24.8 (29.6)
10	62.2 (63.7)	54.6 (60.6)
20	126.6 (125.8)	115.4 (122.6)
30	190.3 (187.8)	176.6 (184.6)
50	316.0 (311.6)	298.8 (308.4)
100	624.8 (620.8)	604.8 (617.6)

[†]The numbers in parentheses refer to 10^{-1} NaCl concentration and those without parentheses to 10^{-3} M NaCl.

roughly the same number of excess counterions (two or three) accumulate around extended and compact configurations; see Table 4. At lower salt, by contrast, the various spatial arrangements cluster into groups with different numbers of associated counterions. In the case of the four-way junction, the greatest build-up of cations occurs around the X-shaped (20°) and distorted tetrahedral forms, which have higher charge densities (i.e. smaller average phosphorus–phosphorus distances) than the other geometries considered here; see Table 1. On the other hand, the smallest accumulation of excess counterions occurs at low salt around the planar cross-shape which has the largest average phosphorus–phosphorus distance of all FWJs. Roughly the same numbers of sodium ions surround the cross-shaped, X-shaped (60°) and tetrahedral forms under the same conditions of ionic strength and chain length. As is evident from Fig. 7, the differences among the configurational states are more pronounced in longer chains and at lower salt. In all cases the number of excess sodium ions grows with increase in chain length and reduction of ionic strength.

The influence of magnesium on the four-way junctions is similar to its effect on kinked and three-way branched DNA structures. Compared to sodium ions, there are fewer excess magnesium ions associated with FWJ structures of the same length and at the same salt concentration. The effect of the junction on counterion build-up is also more pronounced for the smaller FWJs since the number of excess ions (on a per phosphate basis) is larger. For example, at 10^{-3} M $MgCl_2$, the number of excess junction counterions is 0.02 and 0.01 per phosphate group for the cross-shaped FWJ with 10 and 50 bp/arm, respectively. This behavior, which is observed for all geometries and salt (both sodium and magnesium) concentrations, agrees with GCMC predictions [19].

If one envisions FWJ formation from the association of two duplexes (our reference state), then, according to our results, under certain salt conditions and chain lengths there will be an uptake of counterions and thus a change in counterion binding. For instance, for larger FWJs (>50 bp/arm) at low NaCl concentrations, the number of excess sodium ions at the junction is at least 25

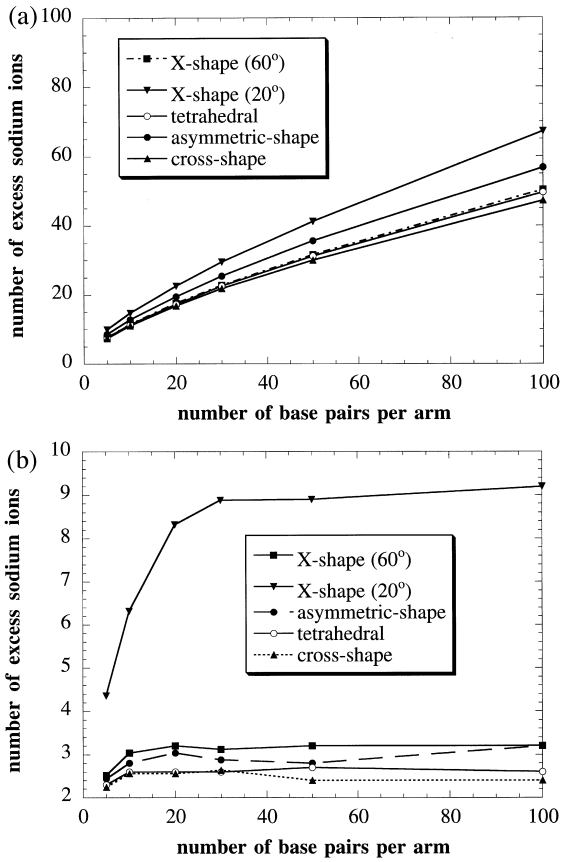

Fig. 7. Chain length dependence of the excess number of sodium ions accumulated around different configurations of four-way DNA junctions in aqueous (a) 10^{-5} M; and (b) 10^{-1} M NaCl solution.

for all geometries. However, at high salt conditions (for both sodium and magnesium) the number of excess counterions is relatively small (0–3) for all configurations, with the exception of the X-shape (20°), which has up to 10 sodium ions. Also, at any NaCl (or $MgCl_2$) concentration the average extent of counterion condensation is not significantly different for many FWJ structures other than the distorted tetrahedral and X-shaped (20°) forms which have higher charge densities.

3.3.1. Comparison with GCMC computations

Fig. 8 compares the numbers of excess sodium ions around the tetrahedral junction predicted from GCMC simulations [19] and our approach

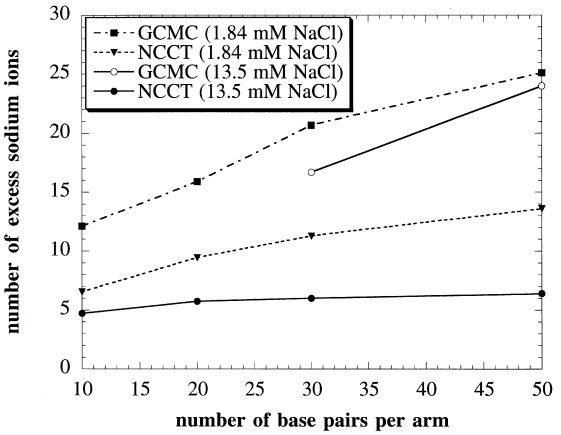

Fig. 8. Comparison of the chain length dependence of the number of excess sodium ions around a tetrahedral DNA junction in aqueous 1.84 and 13.5 mM NaCl solutions, found by grand canonical Monte Carlo (GCMC) simulations and numerical counterion condensation theory (NCCT).

(NCCT) under identical ionic conditions and with the same phosphate spacing. As is evident from the figure, the GCMC study yields a greater number of excess ions around the tetrahedral FWJ with 10–50 bp/arm than the NCCT calculations at both salt concentrations considered (1.84 and 13.5 mM NaCl). The GCMC calculations also find a greater build-up of sodium around the planar cross-shaped junction with 30 bp arms than the NCCT result (21.8 vs. 10.6 sodiums at 1.84 mM salt; data not shown). Both studies predict an increase in the number of excess sodium counterions in longer FWJs, although the increase is less pronounced in the case of NCCT. As noted above in our discussion of kinked DNA, the GCMC analysis defines the excess number of counterions differently from our approach. The GCMC simulations incorporate as 'bound counterions' the non-ideal screening effects of the Debye-Hückel atmosphere, which in our computation affects the free energy but does not supplement the number of bound (condensed) counterions. We believe that our definition of bound counterions as including only the intimately associated condensed layer is more faithful to physical reality.

The two numerical approaches predict nearly the same number of excess sodium ions for tetrahedral and cross-shaped junctions compared to the B-DNA reference. However, our calculations find slightly fewer ions around the cross-shape relative to the tetrahedral structure, whereas the opposite is true according to the GCMC computations. Both methods predict a greater accumulation of sodium around the X-shaped (20°) FWJ with 30 bp/arm (27.5 according to GCMC vs. 18.7 from NCCT at 1.84 mM NaCl) compared to tetrahedral and cross-shaped junctions of the same chain length. The two approaches also find a smaller number of excess sodium ions around the tetrahedral junction at higher salt concentrations. The two studies are thus in good qualitative agreement, predicting the same general ionic strength and chain length dependent trends.

3.3.2. Ionic stability of four-way junctions

The important role of metal ions on the stability of four-way DNA junctions has been well established by many experimental studies [5,20]. Under low salt conditions (or in the absence of metal ions) an extended planar cross-shaped (or square planar) geometry predominates whereas an X-shape (with two acute inter-arm angles of 60°) prevails under high salt conditions or in the presence of magnesium ions [5,20]. As pointed out by others [5,20], there is probably a thermodynamic balance between the ionic and non-ionic (e.g. stacking, base pairing, hydration, etc.) contributions to the total free energy. Since the ionic free energy is larger than the non-ionic free energy at the low salt end, the junction remains extended (or unfolded), whereas the opposite is apparently true at high salt where the compact (or folded) form prevails. Thus, salt induces a conformational transition from a more open or extended geometry at low salt to a more compact or folded geometry (where the average interphosphate distance is smaller) at high salt.

As shown in Fig. 9, which gives ionic stabilities relative to the planar cross-shape, the NCCT data account for the observed ionic effects (both salt concentration and charge) on four-way junctions. At low salt conditions the ionic free energy differences between open and compact configurations are large (as much as 22 kcal/mol between the 20° X-shape and the planar cross at 10^{-5} M NaCl), whereas the ionic stabilities of the X-shape

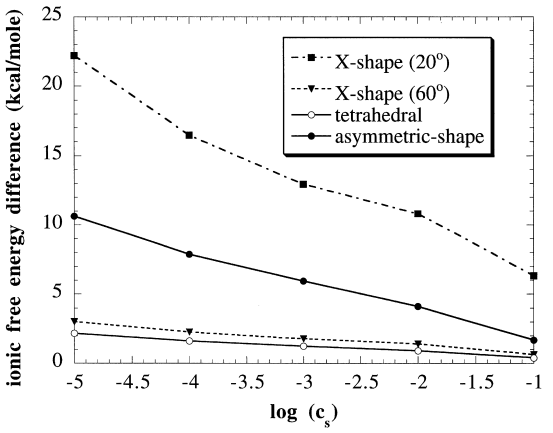

Fig. 9. Ionic free energy differences between various four-way (20 bp arms) DNA junctions and the ideal cross-shaped configuration as a function of the logarithm of the NaCl concentration, c_s.

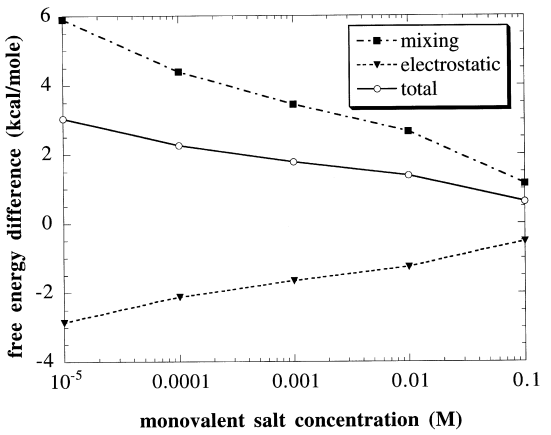

Fig. 10. Salt dependence of the total (ionic), mixing and electrostatic free energy differences between the X-shaped (60°) and ideal cross-shaped configurations of a four-way DNA junction (with 20 bp/arm).

(60°) and cross-shape are comparable (< 0.7 kcal/mol) at high salt. Thus, under low NaCl conditions, more extended geometries, such as the cross-shape, are predicted to occur. With sufficient ion screening (caused by an increase in the salt charge and/or concentration) and the predominance of other energetic factors, the more compact X-shaped geometries become favorable. The order of ionic stability of the different configurations — cross-shape > tetrahedral > X-shape (60°) > distorted tetrahedral > X-shape (20°) — persists over the complete range of chain lengths and salt (both sodium and magnesium) concentration considered here. These differences are most pronounced in long FWJs at low salt.

The ionic free energy differences are quite small when magnesium is the supporting salt (data not shown). For example, the compact X-shape (20°) is only 0.9 kcal/mol less stable than the cross-shape at 10^{-1} M $MgCl_2$. The ionic free energy thus poses no obstacle for the stability of the different geometries. In principle, a variety of different FWJs could co-exist under high $MgCl_2$ concentrations. Other contributions to the total free energy will probably determine which configurations are the most stable.

Fig. 10 shows that the overall dependence of the *total* ionic free energy difference on ionic strength (for the X-shape (60°) relative to the cross-shaped FWJ with 20 bp/arm in NaCl solutions) is mainly dictated by the large *mixing* contribution rather than the smaller *electrostatic* contribution to the total ionic free energy (see Eq. (1) and analysis following it). The entropic mixing contribution, G_{mix}, actually provides a good approximation to the total ionic free energy, whereas the 'electrostatic' term alone does not exhibit the same qualitative trends.

4. Summary and further studies

The present study adds to our understanding of the polyelectrolyte character of kinked and branched DNA and the influence of three-dimensional folding on the electrostatic properties, namely the excess counterions and ionic stabilities, of these chains. The broad range of salt concentrations, chain lengths, and spatial configurations considered here rests upon a fast and simple numerical treatment [22] of classical counterion condensation theory [36] which allows us to extend and generalize observations revealed in past GCMC simulations of representative DNA junctions [19].

While there is only a small build-up of counterions near DNA fragments with small central kinks of $\leq 90°$, a substantial number of ions (> 20) accumulate around all configurations of

large three- and four-way branched DNAs in solutions of low to moderate NaCl concentration. The number of excess counterions drops when the chain length is reduced or when sodium is replaced by magnesium. The build-up of counterions with increasing chain length depends on ionic conditions (both salt concentration and charge) and overall DNA structure. All kinked and branched forms considered here reach an asymptotic limit, where the number of excess ions is invariant to changes in chain length, at moderate to high magnesium concentrations. More open configurations of low charge density — such as slightly kinked duplexes, Y-shaped TWJs and square planar or tetrahedral FWJs — may reach these limits at low salt concentration and/or in the presence of sodium.

Extended configurations tend to accumulate fewer excess counterions and to be ionically favored over more compact forms over a wide range of salt concentration (10^{-5}–10^{-1} M NaCl or $MgCl_2$). In other words, ionic effects favor weakly over strongly kinked duplexes, planar symmetric Y-shaped three-way junctions over asymmetric 'y'-shapes or non-planar trigonal pyramids, and square-planar and tetrahedral four-way junctions over folded X-shapes. The ionic stabilities of the more compact structures increase with increasing salt concentration and approach those of the more open forms at high $MgCl_2$ concentrations.

Neither the present study nor past GCMC calculations can provide insight into the distributions of excess counterions in the vicinity of DNA kinks and junctions, e.g. whether the ions preferentially localize around kink or junction sites, or how the ions redistribute as DNA interconverts between open and closed forms. In principle, the detailed counterion distribution around kinked and branched DNA can be obtained from all-atom molecular dynamics (MD) or Monte Carlo (MC) simulations which explicitly treat the aqueous ionic environment [45–48]. However, state-of-the art MD/MC simulations [47,48] are limited to small nucleic acid fragments (at most $\sim$20 bp) and relatively small volumes of surrounding ions and water molecules. On the other hand, it is possible to gather information about the counterion distributions and ionic stabilities of small kinked and branched DNA structures over a broad range of salt concentrations using less computationally demanding Poisson–Boltzmann calculations, which incorporate details of DNA structure but use a continuum approximation of the solvent/ionic environment [49,50].

Understanding the effects of salt on kinked and branched DNA also requires careful physical characterization of the folding transitions between open and compact forms as a function of salt concentration and charge. Most experimental work to date has focused on the structure rather than the thermodynamics of DNA junctions [51–53] and very little information has been collected about the energetics of salt-induced TWJ and FWJ conformational transitions. New investigations of perfect and bulged branched DNA along the lines of earlier thermodynamics studies of the B $\leftrightarrow$ Z transition [54] could provide a useful starting point for improved theories and computer simulations of the large-scale ion-induced kinking [55] and rearrangement of DNA junctions.

Acknowledgements

We are grateful to Dr A.R. Srinivasan for generation of molecular images in Fig. 1. This work was supported in part by the US Public Health Service under grants GM20861 (WKO) and GM36284 (GSM). Calculations were performed at the Rutgers Center for Computational Chemistry.

References

[1] J.F. Thompson, A. Landy, Nucleic Acids Res. 16 (1988) 9689.
[2] S. Ferrari, V.R. Harley, A. Pontiggia, P.N. Goodfellow, R. Lovell-Badge, M.E. Bianchi, EMBO J. 11 (1992) 4497.
[3] A. Pontiggia, A. Negri, M. Beltrame, M.E. Bianchi, Mol. Microbiol. 7 (1993) 343.
[4] J.J. Love, X. Li, D.A. Case, K. Giese, R. Grosschedl, P. Wright, Nature 376 (1995) 791.
[5] D.M.J. Lilley, R.M. Clegg, Q. Rev. Biophys. 26 (1993) 131.
[6] J.D. Kahn, E. Yun, D.M. Crothers, Nature 368 (1994) 163.

[7] C. Altona, J.A. Pikkemaat, F.J.J. Overmars, Curr. Opin. Struct. Biol. 6 (1996) 305.
[8] P.J. Hagerman, K.M.A. Amiri, Curr. Opin. Struct. Biol. 6 (1996) 317.
[9] C. Altona, J. Mol. Biol. 263 (1996) 568.
[10] N.C. Seeman, N.R. Kallenbach, Ann. Rev. Biophys. Biomol. Struct. 23 (1994) 53.
[11] D.M.J. Lilley, Curr. Opin. Cell Biol. 2 (1990) 464.
[12] F. Jensch, B. Kemper, EMBO J. 5 (1986) 181.
[13] T.R. Broker, A.H. Doermann, Ann. Rev. Genet. 9 (1975) 213.
[14] K.M.A. Amiri, P.J. Hagerman, J. Mol. Biol. 261 (1996) 125.
[15] Z. Shen, P.J. Hagerman, J. Mol. Biol. 241 (1994) 415.
[16] D.R. Duckett, A.I.H. Murchie, D.M.J. Lilley, Cell 83 (1995) 1027.
[17] M.H. Werner, A.M. Gronenborn, G.M. Clore, Science 271 (1996) 778.
[18] R. Klement, in: D.M. Soumpasis, T.M. Jovin (Eds.), Computation of Biomolecular Structures Achievements: Problems and Perspectives, Springer-Verlag, Berlin, 1993, p. 207.
[19] M.C. Olmsted, P.J. Hagerman, J. Mol. Biol. 243 (1994) 919.
[20] D.M.J. Lilley, R.M. Clegg, Ann. Rev. Biophys. Biomol. Struct. 22 (1993) 299.
[21] R.M. Clegg, A.I.H. Murchie, D.M.J. Lilley, Biophys. J. 66 (1994) 99.
[22] M.O. Fenley, G.S. Manning, W.K. Olson, Biopolymers 30 (1990) 1191.
[23] R. Chandrasekaran, S. Arnott, Landolt-Börnstein numerical data and functional relationships in science and Technology, in: W. Saenger (Ed.), New series Group VII: Biophysics (Nucleic Acids, vol. 1, Subvolume b), Springer-Verlag, Berlin, p. 31.
[24] J.A. Pikkemaat, H. van den Elst, J.H. van Boom, C. Altona, Biochemistry 33 (1994) 14896.
[25] S.M. Chen, W.J. Chazin, Biochemistry 33 (1994) 11453.
[26] I.V. Ouporov, N.B. Leontis, Biophys. J. 68 (1995) 266.
[27] A. LeBrun, Z. Shakked, R. Lavery, Proc. Natl. Acad. Sci. U.S.A. 94 (1997) 2993.
[28] H.M. Sobell, C.-C. Tsai, S.C. Gilbert, S.C. Jain, T.D. Sakore, Proc. Natl. Acad. Sci. U.S.A. 73 (1976) 3068.
[29] D.R. Duckett, D.M.J. Lilley, EMBO J. 9 (1990) 1659.
[30] Q. Guo, M. Lu, M.E.A. Churchill, T.D. Tullius, N.R. Kallenbach, Biochemistry 29 (1990) 10927.
[31] M. Lu, Q. Guo, N.R. Kallenbach, Biochemistry 30 (1991) 5815.
[32] F. Stühmeier, J.B. Welch, A.I.H. Murchie, D.M.J. Lilley, R.M. Clegg, Biochemistry 36 (1997) 13530.
[33] L.S. Shlyakhtenko, D. Rekesh, S.M. Lindsay, et al., J. Biomol. Struct. Dyn. 11 (1994) 1175.
[34] D.M.J. Lilley, B. Kemper, Cell 36 (1984) 413.
[35] J.P. Cooper, P.J. Hagerman, Proc. Natl. Acad. Sci. U.S.A. 86 (1989) 7336.
[36] G.S. Manning, Q. Rev. Biophys. 11 (1978) 179.
[37] W.H. Press, B.P. Flannery, S.A. Teukolsky, W.T. Vetterling, Numerical Recipes. The Art of Scientific Computing, Cambridge University Press, Cambridge, 1989, p. 254.
[38] M.T. Record, Jr., C.F. Anderson, T.M. Lohman, Q. Rev. Biophys. 11 (1978) 103.
[39] M.O. Fenley, G.S. Manning, W.K. Olson, J. Phys. Chem. 96 (1992) 3963.
[40] N.B. Leontis, W. Kwok, J.S. Newman, Nucleic Acids Res. 19 (1991) 759.
[41] J.B. Welch, D.R. Duckett, D.M.J. Lilley, Nucleic Acids Res. 21 (1993) 4548.
[42] J.B. Welch, F. Walter, D.M.J. Lilley, J. Mol. Biol. 251 (1995) 507.
[43] F. Stühmeir, D.M.J. Lilley, R.M. Clegg, Biochemistry 36 (1997) 13539.
[44] G.S. Bassi, N.E. Möllegaard, A.I.H. Murchie, E. von Kitzing, D.M.J. Lilley, Nat. Struct. Biol. 2 (1995) 45.
[45] C.A. Laughton, F.J. Luque, M. Orozco, J. Phys. Chem. 99 (1995) 11591.
[46] B. Jayaram, D.L. Beveridge, Ann. Rev. Biophys. Biomol. Struct. 25 (1996) 367.
[47] S. Louise-May, P. Auffinger, E. Westhof, Curr. Opin. Struct. Biol. 6 (1996) 289.
[48] M.A. Young, B. Jayaram, D.L. Beveridge, J. Am. Chem. Soc. 119 (1997) 59.
[49] G.R. Pack, G.A. Garrett, L. Wong, G. Lamm, Biophys. J. 65 (1993) 1363.
[50] V.K. Misra, J.L. Hecht, K.A. Sharp, R.A. Friedman, B. Honig, J. Mol. Biol. 238 (1994) 264.
[51] P.S. Eis, D.P. Millar, Biochemistry 32 (1993) 13852.
[52] M. Yang, D.P. Millar, Biochemistry 35 (1996) 7959.
[53] G. Carlström, W.J. Chazin, Biochemistry 35 (1996) 3534.
[54] F.M. Pohl, T.M. Jovin, J. Mol. Biol. 67 (1972) 375.
[55] W. Han, M. Dlakic, Y.J. Zhu, S.M. Lindsay, R.E. Harrington, Proc. Natl. Acad. Sci. U.S.A. 94 (1997) 10565.